

Manifold GCN: Diffusion-based Convolutional Neural Network for Manifold-valued Graphs

Martin Hanik, Gabriele Steidl, and Christoph von Tycowicz

Abstract—We propose two graph neural network layers for graphs with features in a Riemannian manifold. First, based on a manifold-valued graph diffusion equation, we construct a diffusion layer that can be applied to an arbitrary number of nodes and graph connectivity patterns. Second, we model a tangent multilayer perceptron by transferring ideas from the vector neuron framework to our general setting. Both layers are equivariant with respect to node permutations and isometries of the feature manifold. These properties have been shown to lead to a beneficial inductive bias in many deep learning tasks. Numerical examples on synthetic data as well as on triangle meshes of the right hippocampus to classify Alzheimer’s disease demonstrate the very good performance of our layers.

Index Terms—graph neural networks, manifold-valued features, diffusion, hyperbolic embeddings, shape classification

I. INTRODUCTION

Graph neural networks (GNNs) have gained widespread popularity for the analysis of graph-structured data. They have found applications in various areas, such as bioinformatics [1]–[3], physics [4]–[6], and social sciences [7]–[10]. Important information that GNNs utilize are the features attributed to the graph’s nodes. Here, the vast majority of the GNNs relies on a Euclidean feature space. However, there are many applications where the data lies in a non-flat manifold; for example, on the sphere [11]–[13], the special orthogonal group $SO(3)$ [14], [15], the space of symmetric positive definite (SPD) matrices [16]–[23], the Stiefel manifold [24]–[27], and the Grassmannian manifold [28]–[30]. Also, other Lie Group-valued features are of interest [31]–[36]. So far, there exist only networks that are designed for very specific types of manifolds, such as (products of) spaces of constant curvature [37]–[40] or spaces of SPD matrices [22], [41], [42]. These architectures cannot deal with *general* manifold-valued features.

In this paper, we present a GNN architecture that can work with data from any Riemannian manifold for which geodesics can be efficiently approximated. The core element is a convolution-type layer that discretizes *graph diffusion in manifolds*. We thereby utilize a link between convolution and diffusion processes that has already successfully been used by GNNs for Euclidean data [43]–[45]. Combined with

an explicit solution scheme for the diffusion equation, the *new diffusion layer* exhibits the same local aggregation of features that makes convolution layers so successful [46]. Furthermore, it is equivariant under node permutations as well as isometric transformations of the feature space and, thus, preserves the symmetries inherent to both the base and feature domains. Both properties hold at least approximately for many relationships that deep learning techniques intend to preserve [46]. Indeed, with our layer, we can build networks that are not disturbed, for example, by permutations of a graph’s nodes (symmetry of the base domain) or different feature representations (symmetry of the feature/signal domain). To the best of our knowledge, our layers are the first GNN layers for manifolds that exhibit equivariance under isometries.

Additionally, we propose a novel *tangent multilayer perceptron* that can be seen as a generalization of a fully-connected multilayer perceptron to manifolds, including nonlinearities between layers. It shares the symmetries of the diffusion layer.

We test a network incorporating our novel layers on two different classification tasks: a benchmark on synthetic graphs and the classification of Alzheimer’s disease from triangle meshes of the right hippocampus. Our method outperforms its competition in both cases. We find that our layers lead to fast learning, even with smaller data sets. The code to reproduce the experiments will be made public upon acceptance.

Outline of the paper. We start by recalling related work in Section II. Then, in Section III, we provide the necessary background on Riemannian manifolds and graph Laplacians with manifold-valued features. In Section IV, we introduce our novel diffusion layer and prove its equivariance properties. Our second layer, the tangent multilayer perceptron, is constructed in Section V and shows the same desirable equivariance behavior as the diffusion layer. Both layers are then combined within a generic graph convolutional neural network (GCN) block in Section VI. Section VII contains our numerical results. Finally, a summary and conclusions for future work are given in Section VIII. The appendices contain further theoretical results on the diffusion layer.

II. RELATED WORK

In this section, we review related works and highlight the differences to our contribution. We distinguish between two types of architecture: We start with an overview of GNNs for graphs *with Euclidean features* that discretize a continuous flow in the feature space. We refer to [47] for an overview of the full landscape of Euclidean GNNs. Then, we collect deep learning architectures that can handle *manifold-valued* features.

M. Hanik is with the Freie Universität Berlin, Institute of Mathematics, Arnimallee 14, 14195 Berlin, Germany. E-mail: hanik@zib.de

G. Steidl is with the Technische Universität Berlin, Institute of Mathematics, Straße des 17. Juni 136, 10623 Berlin, Germany. E-mail: steidl@math.tu-berlin.de

C. v. Tycowicz is with the Zuse Institute Berlin, Takustr. 7, 14195 Berlin, Germany. E-mail: vontycowicz@zib.de

Corresponding author: M. Hanik.

A. Flow-based GNNs in the Euclidean Space

Here, two approaches were mainly applied, namely diffusion networks and neural ordinary differential equations.

1) *Diffusion networks*: Diffusion was utilized to construct powerful (graph) convolutional neural networks in [43], [45]. Several papers improved and modified the basic idea. While adaptive support for diffusion-convolutions was proposed in [48], implicit nonlinear diffusion was introduced to capture long-range interactions in [49]. A polynomial filter on the graph Laplacian was used in [50] that corresponds to a multi-scale diffusion equation.

Based on a graph diffusion equation, a broad class of well-performing GNNs was identified in [51], where it was shown in [52] that adding a source term to the equation is useful in certain scenarios. A nonlinear extension of the graph diffusion equation was considered in [53], and many known GNN architectures are instances of the resulting class of GNNs. The framework of [53] also allows the use of non-Euclidean distances for data *encoding*. However, in contrast to our method, this architecture does not treat the features as being intrinsic to a manifold. A different line of work uses diffusion processes in the context of cellular sheaf theory for graph learning [54], [55].

Finally, a diffusion-based architecture, especially for graphs that discretize 2-manifolds (for example, triangular surface meshes), was proposed in [56].

2) *Neural ordinary differential equations*: An approach similar to diffusion-based GNNs is the neural ordinary differential equations (neural ODE) framework [57]. Instead of diffusion-based methods, which treat GNNs as particular instances of the discretization of a *partial* differential equation (in both space and time) [53], it discretizes an underlying ODE. The idea was transferred to graph learning in [58], [59].

B. Deep Neural Networks for Manifold-valued Signals

Here we distinguish between three approaches.

1) *Networks for manifold-valued grids*: ManifoldNet [60] is a convolutional neural network that can take manifold-valued images as input. Convolutions in manifolds are generalized through weighted averaging. However, in contrast to our approach, their layers can only work on *regular grids* as underlying structure and not on general graphs. A similar approach for convolutions using diffusion means was presented in [61].

2) *GNNs for special manifolds*: There have been two main motivations for building GNNs that can deal with manifold-valued features: first, learning from interrelated measurements that take values in some manifold, and second, embedding abstract graphs in curved manifolds to utilize their geometric structure for downstream tasks. Surprisingly, so far, most of the work concentrates on the second aim. The resulting GNNs can only handle data from very restricted classes of manifolds. We discuss the networks and their associated spaces in the following.

There is mounting empirical evidence that embedding graphs in non-Euclidean spaces can help with various tasks. So the authors of [62] observed that a hyperbolic representation

is beneficial when dealing with graphs with a hierarchical structure. Later, products of constant curvature spaces appeared as appropriate embedding spaces for more classes of graphs [63]. In graph representation learning, these observations were further backed up by certain constructions that successfully embed (abstract) graphs into hyperbolic space for downstream tasks [64]–[67]. Other studies showed that other spaces can be better suited than hyperbolic ones when learning, for example classification tasks on wider classes of graphs: While spaces of constant curvature (or products of them) were successfully used in [37]–[40], spaces of non-constant curvature were utilized in the form of Grassmannians [68] and SPD [42], [68] manifolds. In [69], also pseudo-Riemannian manifolds were employed as embedding spaces in the form of pseudo-hyperboloids.

All the above approaches have in common that the *initial* embedding can be chosen or learned freely. This allows for the choice of reference points and the placement of nodes that capture the semantics of input features. Clearly, we do not have this freedom if the data already comes with a fixed embedding. Think, for example, of a network of cities that naturally live on the 2-sphere. The above works usually do not investigate the performance of their networks on data whose embeddings are “far away” from the preferred ones. It must thus be checked additionally if such applications are tackled.

An example where the graphs come with an initial embedding was investigated in [22]. The authors considered SPD-valued graphs that naturally arise from EEG imaging data, and developed network blocks that could navigate the space of SPD matrices with the affine invariant metric. This led to very good classification results.

Unfortunately, all the above GNN architectures have in common that they are not equivariant or invariant under the isometries of the manifold. Whenever the function to be learned (approximately) misses one of these properties, this can lead to suboptimal performance; in such scenarios, non-invariant or non-equivariant networks tend to have many “unnecessary” parameters that make successful training more difficult. We refer to the discussion in [46]) on the curse of dimensionality in machine learning and how shift-invariant/equivariant CNNs helped to overcome it.

3) *Flow-based networks on manifolds*: Neural ODEs were transferred to manifolds in [70], [71]. Besides that, there are also deep learning approaches via discrete [72] and continuous [73], [74] normalizing flows in Riemannian manifolds. For an overview of normalizing flows and its generalizations for Euclidean data, we refer, for example, to [75], [76]. In contrast to our approach, those authors aim to solve a given ODE to learn intricate probability distributions instead of using the ODE to build convolutional layers. The same is true for generative diffusion models [12], [77].

III. BACKGROUND

In this section, we recall the necessary background from differential geometry (see, for example, [78], [79] for more), the notation of graph Laplacians for manifold-valued graphs from [80], and the definitions of invariance and equivariance.

A. Riemannian Geometry

A Riemannian manifold is a d -dimensional manifold¹ M together with a Riemannian metric $\langle \cdot, \cdot \rangle$. The latter assigns to each tangent space $T_p M$ at $p \in M$ an inner product $\langle \cdot, \cdot \rangle_p$ that varies smoothly in p . It induces a norm $\| \cdot \|_p$ on each tangent space $T_p M$ and a distance function $\text{dist} : M \times M \rightarrow \mathbb{R}_{\geq 0}$. Furthermore, it determines the so-called Levi-Civita connection ∇ , which allows for the differentiation of vector fields. For vector fields X and Y on M , we denote the derivative of Y along X by $\nabla_X Y$.

A geodesic is a curve $\gamma : I \rightarrow M$ on an interval $I \subseteq \mathbb{R}$ without acceleration, that is,

$$\nabla_{\gamma'} \gamma' = 0,$$

where $\gamma' := \frac{d}{dt} \gamma$. The manifold M is called complete if every geodesic can be defined on all of \mathbb{R} . In the rest of the paper, we consider only complete, connected Riemannian manifolds M . Locally, geodesics are shortest paths, and the length of a geodesic connecting two points $p, q \in M$ is equal to the distance $\text{dist}(p, q)$. Importantly, every point in M has a so-called normal convex neighborhood $U \subseteq M$ in which any pair $p, q \in U$ can be joined by a unique length-minimizing geodesic $\gamma : [0, 1] \rightarrow M$ with $\gamma(0) = p$ and $\gamma(1) = q$ that lies completely in U . We will need the Riemannian exponential map: For $X \in T_p M$, let γ_X be the geodesic with $\gamma(0) = p$ and $\gamma'(0) = X$. Since geodesics are solutions to ordinary differential equations, there is a neighborhood $W \subset T_p M$ of $0 \in T_p M$ on which the so-called exponential map

$$\exp_p : W \rightarrow M, \quad X \mapsto \gamma_X(1)$$

at p is well defined. It can be shown that \exp_p is a local diffeomorphism. Let $D_p \subset T_p M$ be the maximal neighborhood of $0 \in D_p$, where this is the case, and set $D_p M := \exp_p(D_p)$. Then the inverse $\log_p : D_p M \rightarrow D_p$ of \exp_p is defined and is called the Riemannian logarithm at p . The points q , for which \log_p is not defined, constitute the so-called cut locus of p . Products of Riemannian manifolds are again Riemannian manifolds, where everything works component-wise; this holds in particular for products M^n .

An important class of maps are the so-called isometries (or symmetries) of M . These are diffeomorphisms $\Phi : M \rightarrow M$ that conserve the Riemannian metric, that is, for every $X, Y \in T_p M$, $p \in M$, we have

$$\langle d_p \Phi(X), d_p \Phi(Y) \rangle_{\Phi(p)} = \langle X, Y \rangle_p,$$

where $d_p \Phi : T_p M \rightarrow T_{\Phi(p)} M$ is the differential of Φ at p . Isometries preserve the distance between any two points, map geodesics into geodesics, and map normal convex neighborhoods to normal convex neighborhoods. For every $p \in M$, the exponential and logarithm commute with an isometry Φ as follows:

$$\exp_{\Phi(p)}(d_p \Phi(X)) = \Phi(\exp_p(X)), \quad X \in T_p M, \quad (1)$$

$$d_p \Phi(\log_p(q)) = \log_{\Phi(p)}(\Phi(q)), \quad q \in D_p M. \quad (2)$$

¹Also when not mentioned explicitly, we always assume that manifolds and all maps between manifolds are smooth (that is, infinitely often differentiable).

The set of all isometries of M constitutes the isometry group of M .

Another fundamental property of Riemannian geometry is curvature. The geodesics define the real-valued sectional curvatures K_p that intuitively measure how much surfaces, which are images of planes under \exp_p , bend. Important manifolds of constant sectional curvature $K := K_p \equiv c$ are spheres ($c > 0$), Euclidean spaces ($c = 0$), and hyperbolic spaces ($c < 0$). The curvature has a profound influence on the properties of the manifold. In particular, if M is a so-called Hadamard manifold [78, Ch. 6], that is, a simply connected manifold with non-positive sectional curvature $K_p \leq 0$ everywhere, the whole manifold is a normal convex neighborhood. Apart from Euclidean and hyperbolic spaces, the spaces of symmetric positive definite matrices with the affine invariant metric belong to this class.

B. Graph Laplacian in Manifolds

Let $G = (V, E, w)$ be a directed graph with vertex (node) set $V = \{v_1, \dots, v_n\}$, directed edge set $E \subset V \times V$, and positive edge weights $w : E \rightarrow \mathbb{R}_+$. The ordering of the vertices encodes the direction of the edge, where (v, u) as an edge going from v to u , and we write $u \sim v$ to denote that there exists such an edge.

Starting with the set of functions

$$\mathcal{F}(V, M) := \{f : V \rightarrow M\},$$

we define the set of *admissible* M -valued vertex functions by

$$\mathcal{H}(V, M) := \{f \in \mathcal{F}(V, M) \mid f(u) \in D_{f(v)} M \forall (v, u) \in E\}.$$

The definition ensures that $\log_{f(v)} f(u)$ exists whenever $(v, u) \in E$. Consequently, if $\log_p(q)$ is defined for any $p, q \in M$, then $\mathcal{H}(V, M) = \mathcal{F}(V, M)$. This holds, for instance, for Hadamard manifolds. When a graph G comes with a map $f \in \mathcal{H}(V, M)$, we call f (*vertex*) *features* of G . In this case, we also write $G = (V, E, w, f)$.

For $f \in \mathcal{H}(V, M)$, we denote the disjoint union of tangent spaces at the values of f by

$$T_f M := \bigcup_{v \in V} T_{f(v)} M,$$

and the space of tangent space functions corresponding to f by

$$\mathcal{H}(V, T_f M) := \{F : V \rightarrow T_f M \mid F(v) \in T_{f(v)} M\}.$$

Now the graph Laplacian $\Delta : \mathcal{H}(V, M) \rightarrow \mathcal{H}(V, T_f M)$ is defined for $f \in \mathcal{H}(V, M)$ by

$$\Delta f(v) = - \sum_{u \sim v} w(v, u) \log_{f(v)} f(u) \in T_{f(v)} M, \quad (3)$$

see [80]. If $M = \mathbb{R}^d$, this reduces to a well-known graph Laplacian for Euclidean functions; see, for example, [81].

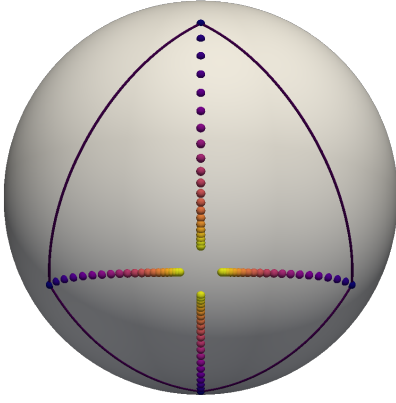


Fig. 1. Diffusion of a rectangle graph on the 2-sphere. Only the edges of the initial graph are shown. Color indicates diffusion time.

C. Equivariance and Invariance

Equivariance and invariance of maps are essential properties of many neural networks. Let S be a set and \mathcal{G} a group with neutral element by e . Assume that \mathcal{G} acts on S (from the left), that is, there is a (left) group action $\rho : \mathcal{G} \times S \rightarrow S$ such that $\rho(e, s) = s$ and $\rho(g, \rho(h, s)) = \rho(gh, s)$. A function $\phi : S \rightarrow \mathbb{R}$ is called invariant with respect to the group action of \mathcal{G} if

$$\phi(\rho(g, s)) = \phi(s)$$

for all $g \in \mathcal{G}$ and $s \in S$. A function $\Phi : S \rightarrow S$ is called equivariant with respect to the group action of \mathcal{G} if

$$\Phi(\rho(g, s)) = \rho(g, \Phi(s))$$

for all $g \in \mathcal{G}$ and $s \in S$. Note that the concatenation of an equivariant and invariant function is again an invariant one.

Equivariance of neural networks under some group operation is usually achieved by stacking, that is, concatenating of layers that are all equivariant themselves. If an invariant network is the goal, several equivariant layers are followed by at least one invariant layer before the final output is generated.

IV. DIFFUSION LAYER

In this section, we introduce a novel diffusion layer. Let $G = (V, E, w, f)$ be a graph with feature map f . We augment f with a time parameter t and consider for $a > 0$, the M -valued graph diffusion equation

$$\begin{cases} \frac{\partial}{\partial t} \tilde{f}(v, t) = -\Delta \tilde{f}(v, t), & v \in V, \quad t \in (0, a), \\ \tilde{f}(v, 0) = f(v), & v \in V. \end{cases} \quad (4)$$

Figure 1 depicts the diffusion of a rectangle graph with constant edge weights. In Appendix A, we show that there always exists a solution to Equation (4) that lives for some time. We also have the following theorem.

Theorem IV.1. *Let $G = (V, E, w, f)$ be a graph with positive weights and features $f \in \mathcal{H}(V, M)$ such that the smallest closed geodesic ball that contains the features of the graph is convex. Assume $\sum_{u \sim v} w(v, u) \leq 1$ for all $v \in V$. Then, Equation (4) has a solution $\tilde{f} : V \times [0, \infty) \rightarrow M$ that is defined for all $t \geq 0$.*

The proof is given in Appendix A.

As discussed in Section II, discrete approximation schemes were used to build neural network layers from diffusion processes in Euclidean space. We will transfer this to manifolds. To this end, we introduce the maps that are needed for the explicit Euler discretization of Equation (4). Motivated by the behavior of the Rectified Linear Unit (ReLU), we define for any $p \in M$, nonlinear activation function $\sigma_p^\alpha : T_p M \rightarrow T_p M$ by

$$\sigma_p^\alpha(X) := \begin{cases} X, & \|X\|_p \geq \alpha, \\ 0, & \text{otherwise.} \end{cases}$$

Then we define for $f \in \mathcal{H}(V, M)$ and $t \geq 0$, the 1-step map $\text{step}_{t, \alpha} : \mathcal{H}(V, M) \rightarrow \mathcal{F}(V, M)$ by

$$(\text{step}_{t, \alpha} f)(v) := \exp_{f(v)} \left(-t \sigma_{f(v)}^\alpha (\Delta f(v)) \right), \quad v \in V.$$

The map $\text{step}_{t, \alpha}$ realizes a “nonlinearly activated” explicit diffusion step of length t of Equation (4). The activation thereby allows only steps that are not shorter than $t\alpha$. Note that since the graph Laplacian is only influenced by a node’s direct neighbors—its so-called *1-hop neighborhood*—, the 1-step map only aggregates information over these neighborhoods.

Remark IV.2. As mentioned before, $\mathcal{H}(V, M) = \mathcal{F}(V, M)$ holds for example in Hadamard manifolds. In this case, $\text{step}_t^\alpha(f)$ cannot lie outside the space of admissible functions. For spaces with positive sectional curvatures, $\text{step}_t^\alpha(f) \notin \mathcal{H}(V, M)$ is in general possible, when two vertices that share an edge lie in their respective cut loci. However, any maximal neighborhood D_p , on which the exponential is invertible, is dense in M (see, for example, [82, Cor. 28.2]). Thus, every cut locus has null measure under the volume measure of the manifold [83, Lem. III.4.4]. Consequently, also in positively curved manifolds, the image $\text{step}_{t, \alpha}(f)$ lies in $\mathcal{H}(V, M)$ except for some exceptional cases.

In Appendix B, we additionally show that the 1-step map always yields admissible features even in positively curved spaces, whenever the data is “local enough” and the step size is not too large. \square

Since numerical approximation schemes usually employ several approximation steps, we extend the 1-step map for $\ell > 1$ and $f \in \mathcal{H}(V, M)$ with $\text{step}_{t, \alpha}^{\ell-1}(f) \in \mathcal{H}(V, M)$ as

$$\text{step}_{t, \alpha}^\ell(f) := \underbrace{\text{step}_{t, \alpha} \circ \dots \circ \text{step}_{t, \alpha}}_{\ell \text{ times}}(f). \quad (5)$$

Again, $\text{step}_{t, \alpha}^\ell$ realizes ℓ “nonlinearly activated” explicit Euler steps of length $t > 0$ for Equation (4). It directly follows that the ℓ -step map aggregates information over ℓ -hop neighborhoods, that is, a nodes new feature is influenced by (the features of) all nodes that are connected to it through a sequence of not more than ℓ edges.

Now we can define our diffusion layer. Let Ω be the set of graphs with vertex features.

Definition IV.3 (Diffusion Layer). For $c \in \mathbb{N}$, let $\mathbf{t} = (t_1, \dots, t_c) \in \mathbb{R}_{\geq 0}^c$ and $\boldsymbol{\alpha} = (\alpha_1, \dots, \alpha_c) \in \mathbb{R}_{\geq 0}^c$. A diffusion layer with $c \geq 1$ channels is a map $\text{Diff}_{\mathbf{t}, \boldsymbol{\alpha}} : \Omega^c \rightarrow \Omega^c$ with

$$\text{Diff}_{\mathbf{t}, \boldsymbol{\alpha}}(G_1, \dots, G_c) = \left((V_i, E_i, w_i, \text{step}_{t_i, \alpha_i}^\ell(f_i)) \right)_{i=1}^c.$$

The diffusion layer takes c graphs as input and diffuses them for certain amounts of time. Thus, it consists of c diffusion “channels.” The diffusion times \mathbf{t} and the step activations $\boldsymbol{\alpha}$ are the learnable parameters. An important property of the new layer is that it can be applied to graphs with varying number of nodes and connectivity patterns. It is also clear that the information aggregation takes place in ℓ -hop neighborhoods. This local aggregation of information is thought to be one of the keys for the success of convolutional (graph) neural networks in many situations [46], [84].

Apart from the already discussed qualities, the diffusion layer possesses the following equivariance properties.

Theorem IV.4. *The diffusion layer is equivariant under node permutations and isometric transformations of the feature manifold.*

Proof. We can restrict ourselves to one channel. The equivariance of the diffusion layer under permutations of the vertex set is already inherent in our formulation as f and Diff are defined on the *unordered* set V . Therefore, if an order is imposed on the vertex set, the node features are sorted accordingly, as well as the output features of the diffusion layer.

Next, we deal with the equivariance under isometries. Let $\Phi : M \rightarrow M$ be an isometry. We must show that transforming features with Φ commutes with applying the diffusion layer:

$$\text{step}_{t, \alpha}^\ell(\Phi \circ f) = \Phi \circ \text{step}_{t, \alpha}^\ell(f).$$

Obviously, it suffices to show the relation for $\ell = 1$. By definition and Equation (2), we have for all $v \in V$ that

$$\begin{aligned} & \text{step}_{t, \alpha}(\Phi \circ f)(v) \\ &= \exp_{\Phi(f(v))} \left(-t\sigma_{\Phi(f(v))}^\alpha \left(\sum_{u \sim v} w(v, u) \log_{\Phi(f(v))} \Phi(f(u)) \right) \right) \\ &= \exp_{\Phi(f(v))} \left(-t\sigma_{\Phi(f(v))}^\alpha \left(\sum_{u \sim v} w(v, u) (d_{f(v)} \Phi)(\log_{f(v)} f(u)) \right) \right), \end{aligned}$$

and by linearity and norm preservation of $d_{f(v)} \Phi$ further

$$\begin{aligned} & \text{step}_{t, \alpha}(\Phi \circ f)(v) \\ &= \exp_{\Phi(f(v))} \left(d_{f(v)} \Phi \left(-t\sigma_{f(v)}^\alpha \left(\sum_{u \sim v} w(v, u) \log_{f(v)} f(u) \right) \right) \right). \end{aligned}$$

Finally, we use (1) to get

$$\begin{aligned} & \text{step}_{t, \alpha}(\Phi \circ f)(v) \\ &= \Phi \left(\exp_{f(v)} \left(-t\sigma_{f(v)}^\alpha \left(\sum_{u \sim v} w(v, u) \log_{f(v)} f(u) \right) \right) \right) \\ &= \Phi \circ \text{step}_{t, \alpha}(f)(v). \end{aligned}$$

This proves the claim. \square

Our diffusion layer is equivariant with respect to the symmetries of the graph and the feature space. As already discussed

earlier, restricting to layers and networks that exhibit this behavior by default is a highly successful ansatz that helps to counter the curse of dimensionality [46]. Thus, the diffusion layer is a highly versatile building block for GNNs.

V. TANGENT MULTILAYER PERCEPTRON

In this section, we introduce a “1x1 convolution” layer that can transform node features and allows to alter the width, that is, the number of channels, of the network. To this end, we transfer ideas from the vector neuron framework [85] to the manifold setting to construct a linear layer on tangent vectors with a subsequent nonlinearity. Due to the latter, the layer can be stacked to increase the depth. Indeed, it works like the well-known multilayer perceptron (MLP).

The layer transforms c_{in} features $f_1, \dots, f_{c_{\text{in}}} \in \mathcal{H}(V, M)$ from c_{in} channels into c_{out} output feature channels $g_1, \dots, g_{c_{\text{out}}} \in \mathcal{H}(V, M)$. To this end, the node features are mapped to a reference tangent space and two sets of linear combinations thereof are learned. One set of vectors is needed to define positive and negative half spaces in the tangent space. The other—output—set is then (nonlinearly) transformed according to the half space they lie in. Finally, the exponential map is applied to transfer the result back to the manifold.

Definition V.1. (Tangent MLP) For $f_1, \dots, f_{c_{\text{in}}} \in \mathcal{H}(V, M)$ and each $v \in V$, let $\bar{f}(v) \in M$ be a point depending on $\mathbf{f}_v := (f_i(v))_{i=1}^{c_{\text{in}}}$ that is equivariant under node permutations and isometries in M . Further assume that $f_1(v), \dots, f_{c_{\text{in}}}(v) \in D_{\bar{f}(v)}M$. The *tangent layer perceptron* with weights ω_j^i, ξ_j^i , $i = 1, \dots, c_{\text{in}}$, $j = 1, \dots, c_{\text{out}}$ and nonlinear scalar function $\sigma : \mathbb{R} \rightarrow \mathbb{R}$ transforms the features of each node into new features $g_1, \dots, g_{c_{\text{out}}} \in \mathcal{H}(V, M)$ in three steps: First, the directions

$$\begin{aligned} X_j(\mathbf{f}_v) &:= \sum_{i=1}^{c_{\text{in}}} \omega_j^i \log_{\bar{f}(v)}(f_i(v)), \\ \tilde{Y}_j(\mathbf{f}_v) &:= \sum_{i=1}^{c_{\text{in}}} \xi_j^i \log_{\bar{f}(v)}(f_i(v)), \\ Y_j(\mathbf{f}_v) &:= \frac{\tilde{Y}_j(\mathbf{f}_v)}{\|\tilde{Y}_j(\mathbf{f}_v)\|_{\bar{f}(v)}} \end{aligned}$$

are computed, and the X_j are orthogonally decomposed with respect to the Y_j as

$$\begin{aligned} X_j^\top(\mathbf{f}_v) &:= \langle X_j(\mathbf{f}_v), Y_j(\mathbf{f}_v) \rangle_{\bar{f}(v)} Y_j(\mathbf{f}_v), \\ X_j^\perp(\mathbf{f}_v) &:= X_j(\mathbf{f}_v) - X_j^\top(\mathbf{f}_v). \end{aligned}$$

Second, the nonlinear scalar function σ is applied

$$Z_j(\mathbf{f}_v) := \frac{\sigma(\|X_j^\top(\mathbf{f}_v)\|_{\bar{f}(v)})}{\|X_j^\top(\mathbf{f}_v)\|_{\bar{f}(v)}} X_j^\top(\mathbf{f}_v) + X_j^\perp(\mathbf{f}_v),$$

and third, the result is transformed back to M via

$$g_j(v; \mathbf{f}_v) := \exp_{\bar{f}(v)}(Z_j(\mathbf{f}_v)).$$

The *tangent multilayer perceptron (tMLP)* with m layers is the concatenation of m tangent linear layers with nonlinearity.

We give some further remarks on the layer.

- Remark V.2.* i) For the reference point \bar{f} , different choices are possible. For example, we can select one of the channel features, that is, $\bar{f}(v) := f_i(v)$ for some $i \in \{1, \dots, c_{\text{in}}\}$, or the Fréchet mean [86] of some of the $(f_i(v))_{i=1}^{c_{\text{in}}}$. The latter is more expensive to compute and harder to differentiate, which is why we use the former choice. Note that the tangent linear layer is *not* equivariant with respect to permutations of the channels. Different from the ordering of the nodes, the ordering of the channels is learned by the model, and we *want* to give the network the freedom to extract information from it.
- ii) Classical options for the nonlinear function σ are the rectified linear unit (ReLU) or leaky ReLU.
- iii) For a tMLP with $m > 1$, it is convenient to use the same reference points in all layers. With this choice, the computation of $g_j(v; \mathbf{f}_v)$ and the applications of the logarithm in the next layer (for $X_j(\mathbf{f}_v)$ and $Y_j(\mathbf{f}_v)$) cancel each other, so these operations can be left away for a higher computational efficiency.
- iv) The arguments from Remark IV.2 concerning the cut locus of a non-Hadamard manifold also apply to the tMLP.
- v) Instead of the tMLP, we could also use sequences of 1D-convolutions from [60]. However, when stacked, the latter require nonlinear activations to guarantee non-collapsibility, and there are no isometry-equivariant manifold-valued activation functions that we are aware of.

The following theorem shows that the tMLP shares the equivariance properties of the diffusion layer.

Theorem V.3. *The tMLP is equivariant under node permutations and isometric transformations of the feature manifold.*

Proof. We show the claim for a single tangent layer perceptron. This directly yields the result for the tMLP since the latter is a concatenation of several linear layers.

The equivariance under permutations of the nodes holds because the weights ω_j^i, ξ_j^i have the same value for every node, and \bar{f} is permuted just like the underlying vertices.

Let $\Phi : M \rightarrow M$ be an isometry. By (2), linearity of $d_{\bar{f}(v)}\Phi$, and since the reference points \bar{f} transforms with the isometry, we obtain with $\Phi \circ \mathbf{f}_v := (\Phi(f_i(v)))_{i=1}^{c_{\text{in}}}$ that

$$\begin{aligned} X_j(\Phi \circ \mathbf{f}_v) &= \sum_{i=1}^{c_{\text{in}}} \omega_j^i \log_{\Phi(\bar{f}(v))} (\Phi(f_i(v))) \\ &= d_{\bar{f}(v)}\Phi \left(\sum_{i=1}^{c_{\text{in}}} \omega_j^i \log_{\bar{f}(v)} (f_i(v)) \right) \\ &= d_{\bar{f}(v)}\Phi(X_j(\mathbf{f}_v)). \end{aligned}$$

Analogously, since $d_{\bar{f}(v)}\Phi$ preserves norms, we obtain

$$\tilde{Y}_j(\Phi \circ \mathbf{f}_v) = d_{\bar{f}(v)}\Phi(\tilde{Y}_j(\mathbf{f}_v)),$$

and further

$$Y_j(\Phi \circ \mathbf{f}_v) = \frac{d_{\bar{f}(v)}\Phi(\tilde{Y}_j(\mathbf{f}_v))}{\|d_{\bar{f}(v)}\Phi(\tilde{Y}_j(\mathbf{f}_v))\|_{\Phi(\bar{f}(v))}} = d_{\bar{f}(v)}\Phi(Y_j(\mathbf{f}_v)).$$

Then, since isometries preserve angles as well, we get

$$\begin{aligned} X_j^\top(\Phi \circ \mathbf{f}_v) &= \langle X_j(\Phi \circ \mathbf{f}_v), Y_j(\Phi \circ \mathbf{f}_v) \rangle_{\Phi \circ \bar{f}(v)} Y_j(\Phi \circ \mathbf{f}_v), \\ &= d_{\bar{f}(v)}\Phi(X_j^\top(\mathbf{f}_v)), \\ X_j^\perp(\Phi \circ \mathbf{f}_v) &= d_{\bar{f}(v)}\Phi(X_j(\mathbf{f}_v) - X_j^\top(\mathbf{f}_v)) \\ &= d_{\bar{f}(v)}\Phi(X_j^\perp(\mathbf{f}_v)). \end{aligned}$$

Thus, we conclude since norms are preserved,

$$\begin{aligned} Z_j(\Phi \circ \mathbf{f}_v) &= \frac{\sigma(\|X_j^\top(\Phi \circ \mathbf{f}_v)\|_{\Phi(\bar{f}(v))})}{\|X_j^\top(\Phi \circ \mathbf{f}_v)\|_{\Phi(\bar{f}(v))}} X_j^\top(\Phi \circ \mathbf{f}_v) \\ &\quad + X_j^\perp(\Phi \circ \mathbf{f}_v) \\ &= d_{\bar{f}(v)}\Phi(Z_j(\mathbf{f}_v)). \end{aligned}$$

Finally, (1) yields

$$\begin{aligned} g_j(v; \Phi \circ \mathbf{f}_v) &= \exp_{\Phi(\bar{f}(v))} (Z_j(\Phi \circ \mathbf{f}_v)) \\ &= \exp_{\Phi(\bar{f}(v))} (d_{\bar{f}(v)}\Phi(Z_j(\mathbf{f}_v))) \\ &= \Phi \left(\exp_{\bar{f}(v)} (Z_j(\mathbf{f}_v)) \right) \\ &= \Phi(g_j(v; \mathbf{f}_v)), \end{aligned}$$

which finishes the proof. \square

VI. MANIFOLD GCN

We now describe a generic graph convolutional neural network (GCN) block to which only the last task-specific layers need to be added for a full architecture: It consists of a sequence

$$\text{Diff} \rightarrow \text{tMLP} \rightarrow \text{Diff} \rightarrow \dots \rightarrow \text{tMLP} \rightarrow \text{Diff} \rightarrow \text{tMLP},$$

in which the numbers of channels of each layer can be chosen freely, as long as the number of output channels of one layer equals the number of input channels of the next. When a graph is fed into the network, c copies of it are given to the first diffusion layer, where c is the number of channels it has. While the diffusion layers aggregate information over the graph, the tMLPs ensure that the architecture is not equivalent to a single diffusion layer (that is, it does not collapse). The tMLPs increase the nonlinearity and allow the network to transfer information between channels.

Later, when we speak of the “depth” of a manifold GCN block, the number of diffusion layers is meant. When all layers have the same number of channels c , we say that the block has “width” c .

When learning scalar outputs (as, for example, in classification), it is usually beneficial to add layers after the manifold GCN block that make the network invariant under node permutations and isometries. We found that the invariant layer from [60, Sec. 2.3] works well; we apply it node-wise and add graph-wise (max- and/or mean-)pooling afterward. While the invariant layer makes the network invariant under isometries [60, Prop. 3], the global pooling operation ensures invariance under node permutations. An MLP with a trailing log-softmax function can finally be added to map, for example, to class probabilities for classification.

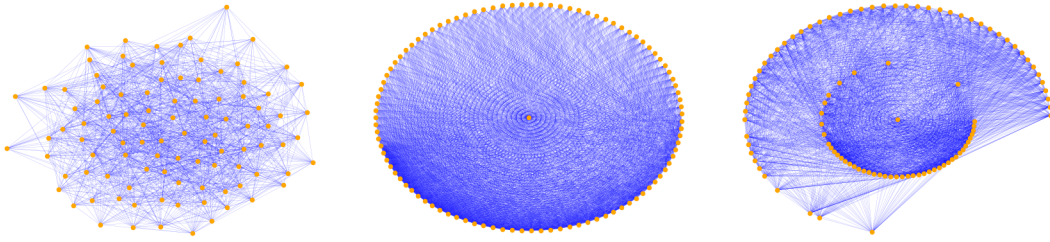


Fig. 2. Graphs created with the Erdős-Rényi (left), Barabasi-Albert (middle), and Watts-Strogatz (right) algorithms.

We found that normalizing the graph weights can boost the performance of GNNs that use a manifold GCN block. The reason, in all likelihood, is that if the step size is too large, the ℓ -step map will be far from the continuous flow, so that the evolution of the graphs becomes “chaotic.” Before feeding a graph $G = (V, E, w, f)$ with $b := \max_{v \in V} \sum_{u \sim v} w(v, u) > 1$ into the network, we thus recommend a global scaling of the weights:

$$\tilde{w} := \frac{w}{b}.$$

Together with “short” initial diffusion times (usually distributed tightly around some $t_0 \in [0, 1]$), we have observed the best performance. Appendix B, which discusses how Diff behaves in certain scenarios, gives further reasons why normalization is helpful.

VII. EXPERIMENTS

The results of our experiments are in this section. We used our manifold GCN in two graph classification tasks.

A. Synthetic Graphs

A benchmark [65] for graph classification algorithms is to let it learn whether a graph was created using the Erdős-Rényi [87], Barabasi-Albert [88], or Watts-Strogatz [89] algorithm. Examples of graphs that were created with each of them are depicted in Figure 2. The authors of [65], [66] showed that classifying from a learned embedding in hyperbolic space is superior to classifying from a Euclidean one. We used our manifold GCN for this task. Since our network can work on arbitrary manifolds, we also compare the hyperbolic space to the SPD space as an embedding space. The latter is thought to be advantageous as it has a more complex geometric structure [42].

1) *Data*: We used differently-sized data sets of graphs built with the three creation algorithms. Each set was balanced; that is, it contained the same number of graphs for each algorithm. Every graph had 100 nodes. The number of edges was chosen (as in [65]) in the following way: For Barabási-Albert graphs, the number of edges to attach from a new node to existing nodes was discrete-uniform distributed between 1 and 200. For Erdős-Rényi, the probability of edge creation was chosen from a uniform distribution on $[0.1, 1]$. For Watts-Strogatz, each node was connected to a discrete-uniform distributed random number between 1 and 200 neighbors in the ring topology, and the probability of rewiring each edge was taken from a uniform distribution on $[0.1, 1]$. All edge-weights were set to $1/100$.

2) *Architecture and Loss*: We used a manifold GCN block of depth 2. The initial flow layer had 5 channels; the following tMLP, which consisted of only one layer and used leaky ReLU as nonlinearity, increased this number to 8. To map to scalar features, we added the invariant layer from [60]. For each node, it calculated the distances to two weighted means, outputting scalar features in 8 channels. Graph-wise max- and mean-pooling were then used for aggregation, and a standard 2-layered MLP with leaky ReLU mapped to the class probabilities using a final log-softmax. The network was trained using the standard cross-entropy loss.

3) *Embedding Manifolds*: In our experiments, we embedded the graphs in hyperbolic and SPD spaces. As the model of hyperbolic space, we used the Lorentz model (see, e.g., [65] for formulas), as it performed best on the given task in [65, Table 1]. When we used the SPD space, we endowed the latter with the affine-invariant metric [86].

4) *Initial Encoding*: For the initial embedding of a graph into hyperbolic space, we used the following options:

- (i) The “degree” embedding from [65]: We assign to each node a one-hot vector X of length 101, the index of the one-entry being the degree of the node. Since the last entry of X is 0, this vector is a tangent vector at the origin $o = [0 \dots 0 1]^T$ of the 100-dimensional Lorentz-hyperboloid \mathcal{H}^{100} . We can then use a (learned) linear function that maps to the tangent space at the origin o_d of a d -dimensional Lorentz space. The final step is then to apply the exponential \exp_{o_d} of the Lorentz model to obtain a feature $\exp_{o_d}(X) \in \mathcal{H}^d$ for the node.
- (ii) The “one-hot” embedding: We choose an order for the graph’s nodes and assign to each node the one-hot vector $X \in T_o \mathcal{H}^{100}$ of length 101 that indicates its place. The final feature is $\exp_o(X)$.

While the first embedding is equivariant under node permutations because of the use of the degree, the one-hot embedding is *not*. Therefore, networks such as HGNN [65] cannot use it without sacrificing invariance under permutations. For our manifold GCN, this is different since two one-hot embeddings can be transformed into each other by a series of rotations (about its symmetry axis) and reflections (about hyperplanes defined by the coordinate axes). Since the latter are isometries of the Lorentz model, the equivariance under isometries of the proposed layers secures the permutation-invariance of the network, even with the one-hot embedding.

For the SPD space, we used a “one-hot” embedding similar to the hyperbolic space. There, the tangent space at the identity

TABLE I
CLASSIFICATION OF SYNTHETIC GRAPHS IN HYPERBOLIC SPACE.

Method # Graphs	Mean F1 Score					# parameters
	90	180	360	1080	2880	
HGNN ($d = 6$)	0.518 \pm 0.133	0.567 \pm 0.085	0.605 \pm 0.060	0.654 \pm 0.040	0.681 \pm 0.042	7053
HGNN ($d = 100$)	0.418 \pm 0.103	0.413 \pm 0.105	0.404 \pm 0.097	0.547 \pm 0.154	0.766 \pm 0.079	161903
Ours (degree)	0.594 \pm 0.114	0.638 \pm 0.084	0.645 \pm 0.062	0.679 \pm 0.037	0.756 \pm 0.046	10429
Ours (one-hot)	0.633 \pm 0.129	0.687 \pm 0.093	0.744 \pm 0.059	0.787 \pm 0.034	0.820 \pm 0.024	429

matrix consists of all symmetric matrices of the same size. We embedded the graphs in the space of 15-by-15 SPD matrices, as this is the smallest such space whose number of free off-diagonal entries is not smaller than the number of nodes. We assigned a symmetric “one-hot” matrix to each node, that is, a symmetric matrix with two one-entries off the diagonal and zero everywhere else. This leads again to permutation-invariant networks for the following reason: We can always transform a one-hot matrix into another via a congruence transformation with the product of two elementary permutation matrices. This represents an isometry since the affine-invariant metric is invariant under congruence with orthogonal matrices [90].

5) *Evaluation and Comparison Methods:* As comparison method, we used the *hyperbolic graph neural network (HGNN)* from [65].² We tried two HGNN models, embedding the graphs in the Lorentz models of 100-dimensional and 6-dimensional hyperbolic space, respectively. We also used two of our networks: one using the degree and the other the one-hot embedding, both in 100-dimensional space.

To compare how well the networks learn with varying amounts of training data, we tested them on data sets with 90, 180, 360, 1800, and 2880 graphs. As measure of classification accuracy, we used the (macro) F1 score. We always split the data set into training, validation, and test sets using a 4:1:1 ratio. The training was done with ADAM. After each epoch, the accuracy on the validation set was computed. Our final model was chosen as the last one with the highest validation score, and its score on the test set was reported. For all but the set with 2880 graphs, we repeated this process 100 times, each time with a new (random) data set; because the standard deviation of the results went down (and the computation times up), we only performed 25 repetitions for the former set.

To also check the performance for large data sets, we created a single data set of 6000 graphs and trained our method with one-hot encoding and the HGNN methods on it. To compare embedding manifolds, we also trained our network using the SPD(15) space. As the evaluation method for this experiment, we chose 3-fold cross-validation.

6) *Software:* All our experiments were performed using Python 3.11. For computations in the hyperbolic and SPD spaces, we used Morphomatics 3.0.2 [91]. The graphs were created with NetworkX 3.2.1 [92] and jraph 0.0.6. The network was implemented in Haiku 0.0.11 using JAX 4.20. The training was done on a GPU using the ADAM implementation of Optax 0.1.7. The parameters were updated using Optax’s incremental

update function with step size 0.1. All experiments with HGNN were performed using the code that is offered by the authors online³, and the software they require.

7) *Parameter Settings:* We used a learning rate of 10^{-3} and trained with balanced batches of size 3 for 60 epochs based on our empirical observations. The computations were performed with double precision.

8) *Results and Discussion:* The average F1 scores and the standard deviations, as well as the number of each network’s trainable parameters, can be found in Table I. For each sample size, manifold GCN with the one-hot embedding performs clearly better than its competitors. This is impressive, especially since it is also the method with the lowest number of trainable parameters. The large difference in the number of parameters for our methods is due to the linear layer in the node embedding. It seems clear that the stronger separation of the embedded nodes helps the network in the learning process. The fact that it is restricted to the degree embedding probably also affects the performance of the HGNN model.

We can also observe that our method performs better when there is less training data. HGNN with a 100-dimensional embedding space starts only to learn when 1080 graphs are in the training set. When the dimension is reduced to 6, it has better performance with small data sets, but the results for bigger sets are worse than with the higher dimension. We think that the better performance for small data sets comes from the inductive bias that we introduce through our isometry-invariant network.

To make sure that the results also hold for the large data sets used in [65], we assembled a set with 6000 graphs and trained on one split. We also included the SPD manifold as the base manifold there. We obtained the following classification accuracies:⁴

- Ours (Hyperbolic one-hot): 0.847,
- Ours (SPD): 0.818,
- HGNN ($d = 6$): 0.690,
- HGNN ($d = 100$): 0.838.

These results confirm our findings. They further indicate that, for this task, the SPD space is not superior to the hyperbolic space.

B. Alzheimer’s disease

Alzheimer’s disease (AD) is a neurodegenerative disorder that is diagnosed more and more often worldwide. Studies

²It performed similarly well as the network from [66] on the task (in particular, reported differences are small and have not been tested for statistical significance). Furthermore, there is a tested code available online.

³<https://github.com/facebookresearch/hgmn>

⁴The difference between our results and those in [65] is not surprising since, there, graphs with up to 500 nodes were used; our results show that the task is harder when there are fewer nodes.

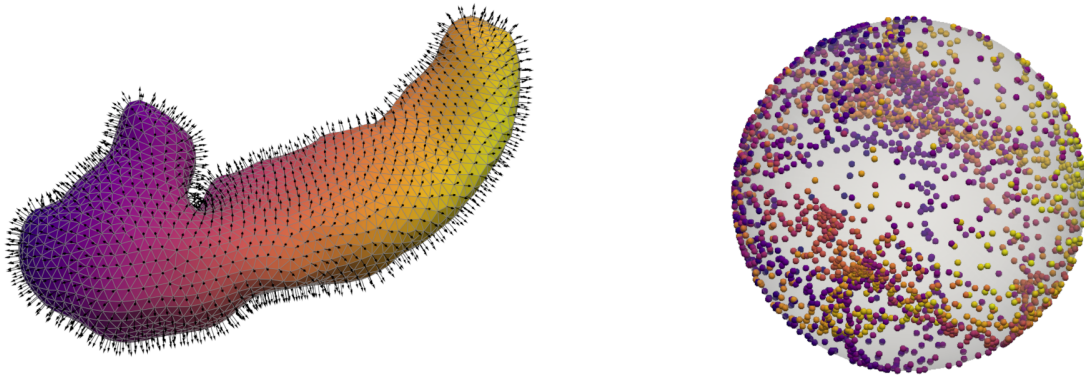


Fig. 3. Hippocampus mesh with vertex normals (left) and the same normals, colored like their footprints, as points on the 2-sphere (right).

showed that AD is characterized by an atrophy pattern of the brain, particularly of the hippocampi; see, for example, [93]. We derived sphere-valued features from digital representations of right hippocampi in the form of normals of triangle meshes. Note that the normals are equivariant under rigid motions of the meshes and invariant under scalings. Since atrophy affects hippocampal volume, we fed this information into the manifold GCN network to classify whether the subject had AD or not.

1) *Data*: For our experiment, we prepared a data set consisting of 60 subjects diagnosed with AD and 60 cognitive normal (CN) controls based on data from the open access Alzheimer’s Disease Neuroimaging Initiative⁵ (ADNI) database. Among others, ADNI provides 1632 magnetic resonance images of brains with segmented hippocampi. In our experiment, we employed the hippocampus meshes derived in [36]. Each mesh was interpreted as a graph. As edge weights, we used the edge weights from the mesh’s cotangent Laplacian. Features were the vertex normals; the latter were computed as the averaged normals of the faces to which the vertex belonged. Due to the equivariance of the normals, our network does not need an alignment of the hippocampi. Nevertheless, the imaging protocol assured a coarse alignment in the coordinate system of the MRI scanner. A visualization of a hippocampus mesh with its normals and their location on the sphere is shown in Figure 3.

2) *Architecture and Loss*: We used a manifold GCN of depth 4 with 16 channels in each layer. Each tMLP consisted of one layer and used leaky ReLU activations. The last layers are the same as in the experiment with synthetic graphs (an invariant layer, a pooling layer, and a final MLP); the only differences are that each has 16 channels and the volume of the hippocampus is appended to the output of the pooling layer. The network was also trained using the standard cross-entropy loss.

3) *Evaluation and Comparison Methods*: We used two different comparison methods. Mesh CNN [94] is a state-of-the-art deep neural network for learning from polygonal meshes. It takes the original meshes as input and combines specialized convolution and pooling layers to predict the class. As the second comparison method, we built a Euclidean

GNN that resembled our proposed network very closely. The manifold GCN block was mimicked using the convolutions from [84] (instead of the diffusion layers) and linear layers (instead of the depth-one tMLPs). We measured the accuracy of the classification, that is, the ratio of correctly classified subjects. We always split the data set into training, validation, and test sets using a 3:1:1 ratio and used ADAM for training. After each epoch, the accuracy on the validation set was computed. For each method, the final model was chosen as the first one with the highest validation score, and its score on the test set was reported.

4) *Software*: We used the same software as in the experiment with the synthetic graphs for our network and its training. Additionally, pyvista 0.42.3 was used to compute the vertex normals and the volumes of the meshes. For MeshCNN, we used the code that is available online.⁶ The Euclidean GNN was built with the graph convolutions provided by jraph 0.0.6.

5) *Parameter Settings*: We used a learning rate of 10^{-3} and trained with batch size 1 for 300 epochs based on our empirical observations. The computations were performed with double precision.

6) *Results and Discussion*: The results of our experiment and the number of trainable parameters for each network are shown in Table II. Our network has the best accuracy among the tested methods. From the performance of Mesh CNN, it becomes clear that the model reduction we perform by considering volume and surface normals instead of the full mesh helps tremendously in this application. Indeed, both methods that utilize only the former information work considerably better. The fact that the Euclidean GNN performs worse shows that the classification is improved by considering the vertex normals as elements of their natural domain, the sphere, and not as elements of the surrounding space.

Importantly, we did not observe antipodal points that were connected with an edge, so no problems with cut loci appeared for our method.

VIII. CONCLUSION

We have presented two new GNN layers for manifold-valued features. They are equivariant under the symmetries

⁵<http://adni.loni.usc.edu/>

⁶<https://ranahanocka.github.io/MeshCNN/>

TABLE II
SHAPE CLASSIFICATION RESULTS.

Method	Mean Accuracy	# parameters
GCN	0.752 ± 0.085	2616
Mesh CNN	0.592 ± 0.073	1320558
Ours (Sphere)	0.765 ± 0.075	2554

of the domain and the feature space of the graph and can be combined to form a highly versatile GNN block that can be used for many deep learning tasks. Contrary to existing GNN methods, our layers can handle data from a wide range of manifolds, which opens up possibilities for deep learning applications on manifold-valued data that could not be tackled with GNNs before.

We applied networks with our new layers to two graph classification tasks, observing very good performances. Tests with little training data suggest that architectures that use it need less training data, probably because of the equivariance properties. This might prove helpful in applications where training data is hard to come by.

Problems that can arise with GNNs are over-squashing and bottleneck phenomena [95]. They lead to situations in which it is very hard to transfer information between distant nodes. A remedy that is presented in [53] is to build layers from diffusion using implicit instead of explicit numerical schemes. This helps to overcome, for example, bottlenecks, as global information is used for an update. This idea can be transferred to our case: future research can focus on making a diffusion layer based on an implicit (Euler) discretization of the diffusion equation. It also seems interesting to test the use of p -Laplacians [80] with $p \neq 2$.

ACKNOWLEDGMENTS

Martin Hanik is supported by the Deutsche Forschungsgemeinschaft (DFG, German Research Foundation) under Germany’s Excellence Strategy—MATH+: The Berlin Mathematics Research Center, EXC-2046/1—project ID: 390685689.

APPENDIX A

PROPERTIES OF THE GRAPH DIFFUSION EQUATION

In this section, we discuss properties of the diffusion equation (4). In particular, we prove Theorem IV.1.

For a graph $G = (V, E, w, f)$ be a graph with (ordered) vertices $V = \{v_1, \dots, v_n\}$, we define

$$\Omega_G := \{ \mathbf{p} = (p_1, \dots, p_n) \in M^n \mid \exists f \in \mathcal{H}(V, M) \text{ such that } f(v_i) = p_i, i = 1, \dots, n \}.$$

This set is open, since every maximal neighborhood $D_p \subseteq T_p M$ in which \exp_p is a diffeomorphism is open. Therefore, Ω_G is a submanifold of M^n (of the same dimension). If M is a Hadamard manifold, then $\Omega_G = M^n$.

Let $J_i \subseteq \{1, \dots, n\}$ denote the index set of the neighbors of v_i . We define the following vector field on Ω_G :

$$\mathbf{p} \mapsto \left(\sum_{j \in J_i} w(v_i, v_j) \log_{p_i} p_j \right)_{i=1}^n. \tag{6}$$

This vector field is smooth in Ω_G , since, away from the cut locus, $\log_p(q)$ is smooth both as a function in p and q ; see, for example, [78, Prop. 18].

Lemma A.1. *i) Equation (4) has a solution if and only if there exists an integral curve $\gamma : [0, a) \rightarrow \Omega_G$ with vector field (6) starting in $(f(v_1), \dots, f(v_n))$. In this case, we have*

$$\gamma_i(t) = \tilde{f}(v_i, t), \quad i = 1, \dots, n, \quad t \in [0, a). \tag{7}$$

ii) There exists $a \in \mathbb{R}_+$ such that Equation (4) has a unique solution on $[0, a)$, which is moreover smooth.

Proof. i) Equation (4) is an autonomous system of n ordinary differential equations on M . Indeed, for $\tilde{f}(v_i, t) := p_i, i = 1, \dots, n$, we find

$$-\Delta \tilde{f}(v_i, t) = \sum_{j \in J_i} w(v_i, v_j) \log_{p_i}(p_j). \tag{8}$$

Therefore, if \tilde{f} solves (4), then we can define the curve γ by (7). Now, Equation (8) implies that the derivative of γ at \mathbf{p} is given by (6), so it is an integral curve of the above vector field. The other direction works by going backwards.

ii) If γ is smooth, then also \tilde{f} . The result now follows from part i) since integral curves of smooth vector fields that start at an arbitrary point and live for a positive amount of time always exist and are smooth [79, Prop. 9.2]. \square

Clearly, if M has a cut locus, then Ω_G is not (geodesically) complete; when the integral curve hits the boundary, it stops. However, if the data is sufficiently localized, this cannot happen, as we show in this appendix.

In the following, a *bounding ball of a graph* is the smallest closed geodesic ball that contains the features of the graph. It exists, for example, if the graph is contained in the maximal neighborhood $D_p M$ of some exponential \exp_p . A closed geodesic ball is convex if any two of its points can be connected by a unique geodesic that never leaves the ball. It is well known that sufficiently small geodesic balls are normal convex neighborhoods [78].

Now we can prove Theorem IV.1, which says that the graph diffusion “lives forever” if the bounding ball of the initial features is convex.

Proof. (Proof of Theorem IV.1)

We know from Lemma (A.1) that there is a solution \tilde{f} that lives at least for some time $a > 0$. We must show that $a = \infty$, and we do so by contradiction.

Assume therefore that $a < \infty$. Then, the Escape Lemma [79, Lem. 9.19] implies that the corresponding integral curve γ leaves every compact subset of Ω_g before it stops at time a . Let \bar{B} be the bounding ball of G . Clearly, \bar{B}^n is a compact subset of Ω_G . We will show that γ cannot leave \bar{B}^n , leading to the desired contradiction.

To this end, let $v \in V$ be a node whose feature lies on the boundary $\partial \bar{B}$ of \bar{B} . Then, because $\sum_{u \sim v} w(v, u) \leq 1$ and because geodesics never leave \bar{B} , the vector $-\Delta f(v)$ either points to the interior of \bar{B} or along its boundary. This is also

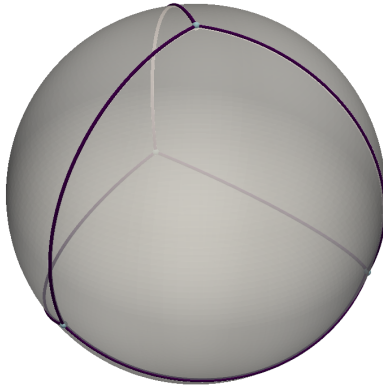


Fig. 4. Stable tetrahedron-graph.

true for any other $\hat{f} \in \mathcal{H}(V, M)$ for which at least one feature lies on $\partial\bar{B}$ and all others in the interior of \bar{B} . Hence, at the boundary $\partial\bar{B}^n$, the vectors (6) point either into the interior of \bar{B}^n or are tangent to $\partial\bar{B}^n$. But then, the integral curve γ cannot leave \bar{B}^n ; see [79, Lem. 9.33]. \square

Example. On a d -dimensional sphere, any graph that is contained in an open hemisphere has a convex bounding ball.

As for the corresponding process in the Euclidean space, constant functions are stable⁷ under the diffusion (4), and many initial configurations will converge towards the same one. An example is shown in Figure 1. Indeed, we conjecture that if a graph’s bounding ball is convex, then its features will always converge to a constant point. However, in some manifolds, there exist non-constant stable functions, as the following example shows.

Example. In the 2-sphere, we can inscribe a regular tetrahedron such that the right-hand side of Equation (3) vanishes at each node, making it stable under diffusion. (For example, when all weights are set to $1/3$.) The graph is shown in Figure 4.

The above example represents a special case of a class of diffusion-stable graphs. Remember that with positive weights $(w_i)_{i=1}^n$ such that $\sum_{i=1}^n w_i = 1$, the weighted Fréchet mean of n points $(p_i)_{i=1}^n \in M^n$ is defined by

$$\text{wFM}\left((w_i)_{i=1}^n, (p_i)_{i=1}^n\right) := \arg \min_{p \in M} \sum_{i=1}^n w_i \text{dist}(p, p_i)^2. \quad (9)$$

Taking the gradient of the sum on the right-hand side of (9) yields, with $\bar{p} := \text{wFM}\left((w_i)_{i=1}^n, (p_i)_{i=1}^n\right)$, the optimality condition

$$\sum_{i=1}^n -2w_i \log_{\bar{p}}(p_i) = 0. \quad (10)$$

This implies the following partial characterization of stable configurations:

⁷A graph with features f is stable under (4) if the solution is independent of t , that is, $\tilde{f}(v, t) = f(v)$ for all $t \in [0, a)$.

Proposition A.2. *If for each node $v \in V$ with neighbors $u_1, \dots, u_{m_v} \in V$ we have*

$$f(v) = \text{wFM}\left(\left(w(v, v_i)\right)_{i=1}^{m_v}, \left(f(v_i)\right)_{i=1}^{m_v}\right),$$

then the graph is stable under diffusion.

Proof. The result follows as the right-hand side of the diffusion equation 4 vanishes using (10). \square

For positively curved spaces, the proposition yields non-constant, stable solutions towards which a diffusion process can flow. In particular, as the hippocampi meshes are topological spheres, the graphs used in this experiment had global support on the 2-sphere. We thus think that the trained neural network observed how the graphs diffused towards a globally supported stable configuration similar to the tetrahedron graph from Figure 4. This makes contacts with the cut locus even more unlikely, since features do not have to “cross an equator” in order to diffuse towards a constant function.

APPENDIX B

THE ℓ -STEP MAP AND NORMAL CONVEX NEIGHBORHOODS

In this appendix, we give some theoretical results on the behavior of the ℓ -step map (5) for localized data.

Proposition B.1. *Let M be a Riemannian manifold, and let $G = (V, E, w, f)$ be a graph with positive weights and features $f \in \mathcal{H}(V, M)$ such that the bounding ball \bar{B} is convex. Assume $\sum_{u \sim v} w(v, u) \leq 1$ for all $v \in V$. Then, there is a maximal $a > 0$ such that for all $t \leq a$*

$$\text{step}_{t, \alpha}^\ell(f)(V) \subset \bar{B}.$$

Proof. Let $v \in V$ be a node whose feature $f(v)$ lies on the boundary of \bar{B} . Then, because $\sum_{u \sim v} w(v, u) \leq 1$, the vector $-\Delta f(v)$ either points to the interior of \bar{B} or along its boundary. Thus, there is a maximal $t_v > 0$ such that $\exp_{f(v)}(-t\Delta f(v)) \in \bar{B}$ for all $t \leq t_v$. Obviously, such a number also exists for vertices whose features are in the interior of \bar{B} . Hence, $a = \max_{v \in V} t_v$. \square

We directly get two corollaries.

Corollary B.2. *Let the assumptions of Proposition B.1 be fulfilled. Then there exists $a > 0$ such that for all $t \leq a$*

$$\text{step}_{t, \alpha}^\ell(f)(v) \in \bar{B}.$$

In particular, every step of the ℓ -step map is well-defined.

By Corollary B.2 a diffusion layer cannot run into trouble with a cut locus, if the bounding ball of an input graph is convex and the time parameter t is smaller than some $a > 0$. The next corollary tells us even more about the behavior of the ℓ -step map.

Corollary B.3. *Let the assumptions of Proposition B.1 be fulfilled. Then there exists $a > 0$ such that for all $t < a$*

$$\begin{aligned} \max_{v, u \in V} \text{dist}(\text{step}_{t, \alpha}^\ell(f)(v), \text{step}_{t, \alpha}^\ell(f)(u)) \\ < \max_{v, u \in V} \text{dist}(f(v), f(u)). \end{aligned}$$

In machine learning applications, we expect that it is preferable when the graphs shrink in diameter (or, at least, do not expand) since most deep learning layers show such a “contractive” behavior; see [60] for a more in-depth discussion on this topic. The corollaries suggest that the diffusion times of a diffusion layer should be initialized close to zero and that the weights of a graph should be normalized, as proposed in Section VI.

REFERENCES

- [1] W. Tornig and R. B. Altman, “Graph convolutional neural networks for predicting drug-target interactions,” *J. Chem. Inf. Model.*, vol. 59, no. 10, pp. 4131–4149, 2019.
- [2] X.-M. Zhang, L. Liang, L. Liu, and M.-J. Tang, “Graph neural networks and their current applications in bioinformatics,” *Front. Genet.*, vol. 12, 2021.
- [3] H.-C. Yi, Z.-H. You, D.-S. Huang, and C. K. Kwoh, “Graph representation learning in bioinformatics: trends, methods and applications,” *Brief. Bioinformatics*, vol. 23, no. 1, p. bbab340, 2022.
- [4] A. Sanchez-Gonzalez, N. Heess, J. T. Springenberg, J. Merel, M. Riedmiller, R. Hadsell, and P. Battaglia, “Graph networks as learnable physics engines for inference and control,” in *International Conference on Machine Learning*. PMLR, 2018, pp. 4470–4479.
- [5] A. Sanchez-Gonzalez, J. Godwin, T. Pfaff, R. Ying, J. Leskovec, and P. Battaglia, “Learning to simulate complex physics with graph networks,” in *Proceedings of the 37th International Conference on Machine Learning*, ser. Proceedings of Machine Learning Research, vol. 119. PMLR, 2020, pp. 8459–8468.
- [6] J. Shlomi, P. Battaglia, and J.-R. Vlimant, “Graph neural networks in particle physics,” *Mach. Learn.: Sci. Technol.*, vol. 2, no. 2, p. 021001, 2020.
- [7] W. Fan, Y. Ma, Q. Li, Y. He, E. Zhao, J. Tang, and D. Yin, “Graph neural networks for social recommendation,” in *The World Wide Web Conference*, 2019, pp. 417–426.
- [8] Y. Wu, D. Lian, Y. Xu, L. Wu, and E. Chen, “Graph convolutional networks with Markov random field reasoning for social spammer detection,” in *Proceedings of the AAAI conference on artificial intelligence*, vol. 34, no. 01, 2020, pp. 1054–1061.
- [9] S. Kumar, A. Mallik, A. Khetarpal, and B. Panda, “Influence maximization in social networks using graph embedding and graph neural network,” *Inf. Sci.*, vol. 607, pp. 1617–1636, 2022.
- [10] L. Wu, Y. Chen, K. Shen, X. Guo, H. Gao, S. Li, J. Pei, and B. Long, “Graph neural networks for natural language processing: A survey,” *Found. Trends Mach. Learn.*, vol. 16, no. 2, pp. 119–328, 2023.
- [11] N. I. Fisher, T. Lewis, and B. J. Embleton, *Statistical analysis of spherical data*. Cambridge, UK: Cambridge University Press, 1993.
- [12] V. De Bortoli, E. Mathieu, M. Hutchinson, J. Thornton, Y. W. Teh, and A. Doucet, “Riemannian score-based generative modelling,” *Adv. Neural Inf. Process. Syst.*, vol. 35, pp. 2406–2422, 2022.
- [13] E. Nava-Yazdani, F. Ambellan, M. Hanik, and C. von Tycowicz, “Sasaki metric for spline models of manifold-valued trajectories,” *Comput. Aided Geom. Des.*, p. 102220, 2023.
- [14] R. Bergmann, R. H. Chan, R. Hielscher, J. Persch, and G. Steidl, “Restoration of manifold-valued images by half-quadratic minimization,” *Inverse Probl. Imaging*, vol. 10, no. 2, pp. 281–304, 2016.
- [15] M. Gräf, S. Neumayer, R. Hielscher, G. Steidl, M. Liesegang, and T. Beck, “An optical flow model in electron backscatter diffraction,” *SIAM J. Imaging Sci.*, vol. 15, no. 1, pp. 228–260, 2022.
- [16] A. Cherian and S. Sra, “Positive definite matrices: data representation and applications to computer vision,” *Algorithmic Advances in Riemannian Geometry and Applications: For Machine Learning, Computer Vision, Statistics, and Optimization*, pp. 93–114, 2016.
- [17] P. T. Fletcher and S. Joshi, “Riemannian geometry for the statistical analysis of diffusion tensor data,” *Signal Process.*, vol. 87, no. 2, pp. 250–262, 2007.
- [18] K. You and H.-J. Park, “Re-visiting Riemannian geometry of symmetric positive definite matrices for the analysis of functional connectivity,” *NeuroImage*, vol. 225, p. 117464, 2021.
- [19] X. Pennec, “Manifold-valued image processing with SPD matrices,” in *Riemannian geometric statistics in medical image analysis*. Elsevier, 2020, pp. 75–134.
- [20] M. Hanik, M. A. Demirtaş, M. A. Gharsallaoui, and I. Rekek, “Predicting cognitive scores with graph neural networks through sample selection learning,” *Brain Imaging Behav.*, pp. 1–16, 2021.
- [21] E. Wong, J. S. Anderson, B. A. Zielinski, and P. T. Fletcher, “Riemannian regression and classification models of brain networks applied to autism,” in *Connectomics in NeuroImaging: Second International Workshop, CNI 2018, Held in Conjunction with MICCAI 2018, Granada, Spain, September 20, 2018, Proceedings 2*. Springer, 2018, pp. 78–87.
- [22] C. Ju and C. Guan, “Graph neural networks on SPD manifolds for motor imagery classification: A perspective from the time-frequency analysis,” *IEEE Trans. Neural Netw. Learn. Syst.*, pp. 1–15, 2023.
- [23] F. Nerrise, Q. Zhao, K. L. Poston, K. M. Pohl, and E. Adeli, “An explainable geometric-weighted graph attention network for identifying functional networks associated with gait impairment,” in *International Conference on Medical Image Computing and Computer-Assisted Intervention*. Springer, 2023, pp. 723–733.
- [24] L. Lin, V. Rao, and D. Dunson, “Bayesian nonparametric inference on the Stiefel manifold,” *Stat. Sin.*, pp. 535–553, 2017.
- [25] R. Chakraborty and B. C. Vemuri, “Statistics on the Stiefel manifold: Theory and applications,” *Ann. Stat.*, vol. 47, no. 1, pp. 415–438, 2019.
- [26] J. Chen, G. Han, H. Cai, D. Yang, P. J. Laurienti, M. Styner, and G. Wu, “Learning common harmonic waves on Stiefel manifold—a new mathematical approach for brain network analyses,” *IEEE Trans. Med. Imaging*, vol. 40, no. 1, pp. 419–430, 2020.
- [27] C. Mantoux, B. Couvy-Duchesne, F. Cacciamani, S. Epelbaum, S. Durleman, and S. Allasonnière, “Understanding the variability in graph data sets through statistical modeling on the Stiefel manifold,” *Entropy*, vol. 23, no. 4, p. 490, 2021.
- [28] P. Turaga, A. Veeraraghavan, A. Srivastava, and R. Chellappa, “Statistical computations on Grassmann and Stiefel manifolds for image and video-based recognition,” *IEEE Trans. Pattern Anal. Mach. Intell.*, vol. 33, no. 11, pp. 2273–2286, 2011.
- [29] Z. Huang, R. Wang, S. Shan, and X. Chen, “Projection metric learning on Grassmann manifold with application to video based face recognition,” in *Proceedings of the IEEE Conference on Computer Vision and Pattern Recognition*, 2015, pp. 140–149.
- [30] Z. Huang, J. Wu, and L. Van Gool, “Building deep networks on Grassmann manifolds,” in *Proceedings of the AAAI Conference on Artificial Intelligence*, vol. 32, no. 1, 2018.
- [31] F. Park, J. Bobrow, and S. Ploen, “A Lie group formulation of robot dynamics,” *Int. J. Rob. Res.*, vol. 14, no. 6, pp. 609–618, 1995.
- [32] M. Hanik, H.-C. Hege, and C. von Tycowicz, “Bi-invariant dissimilarity measures for sample distributions in Lie groups,” *SIAM J. Math. Data Sci.*, vol. 4, no. 4, pp. 1223–1249, 2022.
- [33] R. Vemulapalli, F. Arrate, and R. Chellappa, “Human action recognition by representing 3D skeletons as points in a Lie group,” in *Proceedings of the IEEE Conference on Computer Vision and Pattern Recognition*, 2014, pp. 588–595.
- [34] R. Vemulapalli and R. Chellapa, “Rolling rotations for recognizing human actions from 3D skeletal data,” in *Proceedings of the IEEE Conference on Computer Vision and Pattern Recognition*, 2016, pp. 4471–4479.
- [35] C. von Tycowicz, F. Ambellan, A. Mukhopadhyay, and S. Zachow, “An efficient Riemannian statistical shape model using differential coordinates,” *Med. Image Anal.*, vol. 43, pp. 1–9, 2018.
- [36] F. Ambellan, S. Zachow, and C. von Tycowicz, “Rigid motion invariant statistical shape modeling based on discrete fundamental forms,” *Med. Image Anal.*, vol. 73, p. 102178, 2021.
- [37] G. Bachmann, G. Bécigneul, and O. Ganea, “Constant curvature graph convolutional networks,” in *International Conference on Machine Learning*. PMLR, 2020, pp. 486–496.
- [38] S. Zhu, S. Pan, C. Zhou, J. Wu, Y. Cao, and B. Wang, “Graph geometry interaction learning,” *Adv. Neural Inf. Process. Syst.*, vol. 33, pp. 7548–7558, 2020.
- [39] L. Sun, Z. Zhang, J. Ye, H. Peng, J. Zhang, S. Su, and S. Y. Philip, “A self-supervised mixed-curvature graph neural network,” in *Proceedings of the AAAI Conference on Artificial Intelligence*, vol. 36, no. 4, 2022, pp. 4146–4155.
- [40] C. Deng, F. Xu, J. Ding, L. Fu, W. Zhang, and X. Wang, “Fmgnn: Fused manifold graph neural network,” 2023.
- [41] Z. Huang and L. Van Gool, “A Riemannian network for SPD matrix learning,” in *Proceedings of the AAAI conference on artificial intelligence*, vol. 31, no. 1, 2017, pp. 2036–2042.
- [42] W. Zhao, F. Lopez, M. J. Riestenberg, M. Strube, D. Taha, and S. Trettel, “Modeling graphs beyond hyperbolic: Graph neural networks in symmetric positive definite matrices,” in *Joint European Conference on*

- Machine Learning and Knowledge Discovery in Databases.* Springer, 2023, pp. 122–139.
- [43] J. Atwood and D. Towsley, “Diffusion-convolutional neural networks,” *Adv. Neural Inf. Process. Syst.*, vol. 29, pp. 2001–2009, 2016.
- [44] Y. Li, R. Yu, C. Shahabi, and Y. Liu, “Diffusion convolutional recurrent neural network: Data-driven traffic forecasting,” in *International Conference on Learning Representations*, 2018.
- [45] J. Gasteiger, S. Weissenberger, and S. Günnemann, “Diffusion improves graph learning,” *Adv. Neural Inf. Process. Syst.*, vol. 32, pp. 13 366–13 378, 2019.
- [46] M. M. Bronstein, J. Bruna, T. Cohen, and P. Veličković, “Geometric deep learning: Grids, groups, graphs, geodesics, and gauges,” *arXiv preprint arXiv:2104.13478*, 2021.
- [47] Z. Wu, S. Pan, F. Chen, G. Long, C. Zhang, and S. Y. Philip, “A comprehensive survey on graph neural networks,” *IEEE Trans. Neural Netw. Learn. Syst.*, vol. 32, no. 1, pp. 4–24, 2020.
- [48] J. Zhao, Y. Dong, M. Ding, E. Kharlamov, and J. Tang, “Adaptive diffusion in graph neural networks,” *Adv. Neural Inf. Process. Syst.*, vol. 34, pp. 23 321–23 333, 2021.
- [49] Q. Chen, Y. Wang, Y. Wang, J. Yang, and Z. Lin, “Optimization-induced graph implicit nonlinear diffusion,” in *International Conference on Machine Learning*. PMLR, 2022, pp. 3648–3661.
- [50] R. Liao, Z. Zhao, R. Urtasun, and R. S. Zemel, “Lanczosnet: Multi-scale deep graph convolutional networks,” *arXiv preprint arXiv:1901.01484*, 2019.
- [51] B. Chamberlain, J. Rowbottom, M. I. Gorinova, M. Bronstein, S. Webb, and E. Rossi, “Grand: Graph neural diffusion,” in *International Conference on Machine Learning*. PMLR, 2021, pp. 1407–1418.
- [52] M. Thorpe, T. M. Nguyen, H. Xia, T. Strohmer, A. Bertozzi, S. Osher, and B. Wang, “Grand++: Graph neural diffusion with a source term,” in *International Conference on Learning Representations*, 2021.
- [53] B. Chamberlain, J. Rowbottom, D. Eynard, F. Di Giovanni, X. Dong, and M. Bronstein, “Beltrami flow and neural diffusion on graphs,” *Adv. Neural Inf. Process. Syst.*, vol. 34, pp. 1594–1609, 2021.
- [54] J. Hansen and T. Gebhart, “Sheaf neural networks,” *arXiv preprint arXiv:2012.06333*, 2020.
- [55] C. Bodnar, F. Di Giovanni, B. Chamberlain, P. Liò, and M. Bronstein, “Neural sheaf diffusion: A topological perspective on heterophily and oversmoothing in GNNs,” *Adv. Neural Inf. Process. Syst.*, vol. 35, pp. 18 527–18 541, 2022.
- [56] N. Sharp, S. Attaiki, K. Crane, and M. Ovsjanikov, “Diffusionnet: Discretization agnostic learning on surfaces,” *ACM Trans. Graph.*, vol. 41, no. 3, pp. 1–16, 2022.
- [57] R. T. Chen, Y. Rubanova, J. Bettencourt, and D. K. Duvenaud, “Neural ordinary differential equations,” *Adv. Neural Inf. Process. Syst.*, vol. 31, 2018.
- [58] M. Poli, S. Massaroli, J. Park, A. Yamashita, H. Asama, and J. Park, “Graph neural ordinary differential equations,” *arXiv preprint arXiv:1911.07532*, 2019.
- [59] L.-P. Khonneux, M. Qu, and J. Tang, “Continuous graph neural networks,” in *International Conference on Machine Learning*. PMLR, 2020, pp. 10 432–10 441.
- [60] R. Chakraborty, J. Bouza, J. Manton, and B. C. Vemuri, “Manifoldnet: A deep neural network for manifold-valued data with applications,” *IEEE Trans. Pattern Anal. Mach. Intell.*, vol. 44, no. 2, pp. 799–810, 2020.
- [61] S. Sommer and A. Bronstein, “Horizontal flows and manifold stochastics in geometric deep learning,” *IEEE Trans. Pattern Anal. Mach. Intell.*, vol. 44, no. 2, pp. 811–822, 2020.
- [62] D. Krioukov, F. Papadopoulos, M. Kitsak, A. Vahdat, and M. Boguná, “Hyperbolic geometry of complex networks,” *Phys. Rev. E*, vol. 82, no. 3, p. 036106, 2010.
- [63] A. Gu, F. Sala, B. Gunel, and C. Ré, “Learning mixed-curvature representations in product spaces,” in *International Conference on Learning Representations*, 2019.
- [64] I. Chami, Z. Ying, C. Ré, and J. Leskovec, “Hyperbolic graph convolutional neural networks,” *Adv. Neural Inf. Process. Syst.*, vol. 32, 2019.
- [65] Q. Liu, M. Nickel, and D. Kiela, “Hyperbolic graph neural networks,” *Adv. Neural Inf. Process. Syst.*, vol. 32, 2019.
- [66] J. Dai, Y. Wu, Z. Gao, and Y. Jia, “A hyperbolic-to-hyperbolic graph convolutional network,” in *Proceedings of the IEEE/CVF Conference on Computer Vision and Pattern Recognition*, 2021, pp. 154–163.
- [67] Y. Zhang, X. Wang, C. Shi, N. Liu, and G. Song, “Lorentzian graph convolutional networks,” in *Proceedings of the Web Conference 2021*. New York: Association for Computing Machinery, 2021, pp. 1249–1261.
- [68] C. Cruceru, G. Bécigneul, and O.-E. Ganea, “Computationally tractable Riemannian manifolds for graph embeddings,” in *Proceedings of the AAAI Conference on Artificial Intelligence*, vol. 35, no. 8, 2021, pp. 7133–7141.
- [69] B. Xiong, S. Zhu, N. Potyka, S. Pan, C. Zhou, and S. Staab, “Pseudo-Riemannian graph convolutional networks,” *Adv. Neural Inf. Process. Syst.*, vol. 35, pp. 3488–3501, 2022.
- [70] A. Lou, D. Lim, I. Katsman, L. Huang, Q. Jiang, S. N. Lim, and C. M. De Sa, “Neural manifold ordinary differential equations,” *Adv. Neural Inf. Process. Syst.*, vol. 33, pp. 17 548–17 558, 2020.
- [71] I. Katsman, E. M. Chen, S. Holakere, A. Asch, A. Lou, S.-N. Lim, and C. D. Sa, “Riemannian residual neural networks,” in *Thirty-seventh Conference on Neural Information Processing Systems*, 2023.
- [72] D. J. Rezende, G. Papamakarios, S. Racaniere, M. Albergo, G. Kanwar, P. Shanahan, and K. Cranmer, “Normalizing flows on tori and spheres,” in *International Conference on Machine Learning*. PMLR, 2020, pp. 8083–8092.
- [73] E. Mathieu and M. Nickel, “Riemannian continuous normalizing flows,” *Adv. Neural Inf. Process. Syst.*, vol. 33, pp. 2503–2515, 2020.
- [74] N. Rozen, A. Grover, M. Nickel, and Y. Lipman, “Moser flow: Divergence-based generative modeling on manifolds,” *Adv. Neural Inf. Process. Syst.*, vol. 34, pp. 17 669–17 680, 2021.
- [75] P. Hagemann, J. Hertrich, and G. Steidl, “Generalized normalizing flows via Markov chains,” in *Non-local data interactions: foundations and applications*. Cambridge, UK: Cambridge University Press, 2023.
- [76] L. Ruthotto and E. Haber, “An introduction to deep generative modeling,” *DMV Mitteilungen*, vol. 44, no. 3, pp. 1–24, 2021.
- [77] J. Thornton, M. Hutchinson, E. Mathieu, V. De Bortoli, Y. W. Teh, and A. Doucet, “Riemannian diffusion Schrödinger bridge,” *arXiv preprint arXiv:2207.03024*, 2022.
- [78] P. Petersen, *Riemannian Geometry*. Berlin: Springer, 2006.
- [79] J. M. Lee, *Introduction to Smooth Manifolds*. Berlin: Springer, 2012.
- [80] R. Bergmann and D. Tenbrinck, “A graph framework for manifold-valued data,” *SIAM J. Imaging Sci.*, vol. 11, no. 1, pp. 325–360, 2018.
- [81] G. Gilboa and S. Osher, “Nonlocal operators with applications to image processing,” *SIAM Multiscale. Model. Simul.*, vol. 7(3), pp. 1005–1028, 2008.
- [82] M. M. Postnikov, *Geometry VI: Riemannian Geometry*. Berlin: Springer, 2013.
- [83] T. Sakai, *Riemannian geometry*. Providence, USA: American Mathematical Soc., 1996.
- [84] T. N. Kipf and M. Welling, “Semi-supervised classification with graph convolutional networks,” in *International Conference on Learning Representations*, 2017.
- [85] C. Deng, O. Litany, Y. Duan, A. Poulenard, A. Tagliasacchi, and L. J. Guibas, “Vector neurons: A general framework for SO(3)-equivariant networks,” in *Proceedings of the IEEE/CVF International Conference on Computer Vision*, 2021, pp. 12 200–12 209.
- [86] X. Pennec, “Intrinsic statistics on Riemannian manifolds: basic tools for geometric measurements,” *J. Math. Imaging Vis.*, vol. 25, pp. 127–154, 2006.
- [87] P. Erdős and A. Rényi, “On the evolution of random graphs,” *Publication of the Mathematical Institute of the Hungarian Academy of Sciences*, vol. 5, no. 1, pp. 17–60, 1960.
- [88] A.-L. Barabási and R. Albert, “Emergence of scaling in random networks,” *Science*, vol. 286, no. 5439, pp. 509–512, 1999.
- [89] D. J. Watts and S. H. Strogatz, “Collective dynamics of ‘small-world’ networks,” *Nature*, vol. 393, no. 6684, pp. 440–442, 1998.
- [90] Y. Thanwerdas and X. Pennec, “O(n)-invariant Riemannian metrics on SPD matrices,” *Linear Algebra Appl.*, vol. 661, pp. 163–201, 2023.
- [91] F. Ambellan, M. Hanik, and C. von Tycowicz, “Morphomatics: Geometric morphometrics in non-Euclidean shape spaces,” 2021, <https://morphomatics.github.io/>.
- [92] A. A. Hagberg, D. A. Schult, and P. J. Swart, “Exploring network structure, dynamics, and function using networkx,” in *Proceedings of the 7th Python in Science Conference*, G. Varoquaux, T. Vaught, and J. Millman, Eds., Pasadena, CA USA, 2008, pp. 11–15.
- [93] S. G. Mueller, N. Schuff, K. Yaffe, C. Madison, B. Miller, and M. W. Weiner, “Hippocampal atrophy patterns in mild cognitive impairment and Alzheimer’s disease,” *Hum. Brain Mapp.*, vol. 31, no. 9, pp. 1339–1347, 2010.
- [94] R. Hanocka, A. Hertz, N. Fish, R. Giryes, S. Fleishman, and D. Cohen-Or, “MeshCNN: A network with an edge,” *ACM Trans. Graph.*, vol. 38, no. 4, 2019.
- [95] U. Alon and E. Yahav, “On the bottleneck of graph neural networks and its practical implications,” in *International Conference on Learning Representations*, 2021.